

Paschen Jumps in Little Red Dots: Evidence for Nebular Continua

Albert Sneppen^{1,2}, James H. Matthews³, Darach Watson^{1,2}, Alex J. Cameron^{1,2}, Stuart A. Sim⁴,
Joris Witstok^{1,2}, Gabriel B. Brammer^{1,2}, Kasper E. Heintz^{1,2}, Georgios Nikopoulos^{1,2}

¹ Cosmic Dawn Center (DAWN)

² Niels Bohr Institute, University of Copenhagen, Jagtvej 128, DK-2200, Copenhagen N, Denmark

³ Astrophysics, Department of Physics, University of Oxford, Oxford OX1 3RH, UK

⁴ School of Mathematics and Physics, Astrophysics Research Centre, Queen's University Belfast, Belfast, United Kingdom

Received date / Accepted date

ABSTRACT

“Little Red Dots” (LRDs) are broad-line sources at high redshift, initially identified by their compact morphologies, red colours and prominent Balmer breaks. The origin of their optical-to-near-infrared continua is debated, with proposed explanations ranging from direct recombination emission to thermalised blackbodies from stellar-like atmospheres. Here we report evidence for Paschen jumps in a subset of LRDs, consistent with free-bound recombination to hydrogen $n = 3$. The Paschen and Brackett continuum shapes across the sample are consistent with minimally reddened emission from low-temperature gas with $T_e \lesssim 10\,000$ K, while the presence of Paschen jump signatures limits scenarios in which the emission is thermalised. Further, the extreme $H\alpha$ equivalent widths and the tight observed correlation between $H\alpha$ and the continuum follow naturally if both originate in recombination emission. This provides an observational upper limit on the contribution of any direct AGN accretion component and any stellar-atmosphere-like component, as well as on the fraction of line emission that can be thermalised as it traverses the cocoon. Ultimately, nebular radiative-transfer models provide a self-consistent explanation of the continuum, line strengths and line profiles without requiring multiple separately fitted components.

1. Introduction

The population of compact, extremely red sources called ‘little red dots’ (LRDs), apparently common at high redshift, has been one of the major discoveries of *JWST*. They are characterised by broad hydrogen and helium permitted lines (Matthee et al. 2024; Greene et al. 2024; Kocevski et al. 2024; Killi et al. 2024) as well as high surface brightness (Kokorev et al. 2024; de Graaff et al. 2025a), initially suggesting virial motion around, and accretion onto, a supermassive black hole. However, they exhibit spectral signatures more commonly associated with stars and transients. These include i) Balmer breaks and Balmer-line absorptions from large columns of hydrogen gas with significant $n = 2$ populations (Setton et al. 2024; Inayoshi & Maiolino 2025), ii) line broadening dominated by electron-scattering (Rusakov et al. 2026; Chang et al. 2025; Torralba et al. 2025) and iii) red spectral continua with shapes reminiscent of blackbodies (Kido et al. 2025; Liu et al. 2025; de Graaff et al. 2025b; Sun et al. 2026).

These features collectively hint at a dense, stratified cocoon or envelope surrounding the supermassive black hole, containing both predominantly ionised and predominantly neutral regions that reprocess the accretion power into red emission. Further, this cocoon would potentially suppress radio and X-ray emission, which are typically undetected (Maiolino et al. 2025; Juodžbalis et al. 2024; Rusakov et al. 2026), the high densities may naturally explain observed LRD line ratios deviating from Case-B recombination (Nikopoulos et al. 2025; D’Eugenio et al. 2025a; Yan et al. 2025), and the cocoon can reach temperatures < 3000 K, permitting observed LRD molecular features of water absorption (Wang et al. 2026). This motivates detailed radiative transfer modelling to capture this new physical regime and explain the puzzling nature of the red optical to near-infrared continuum (Rusakov et al. 2026; Chang et al. 2025; Sneppen et al. 2026).

Interpretations of this red continuum include accretion disc emission associated with AGN attenuated by large gas columns (Inayoshi & Maiolino 2025), recombination emission of the gas cocoon (Rusakov et al. 2026; Sneppen et al. 2026), Hayashi-like gas envelopes (Kido et al. 2025; Begelman & Dexter 2025) and fully reprocessed, thermalised blackbody emission from dense gas in the so-called ‘black hole star’-model (Naidu et al. 2025; de Graaff et al. 2025a,b; Sun et al. 2026; Liu et al. 2026). While these proposed explanations draw upon the same idea of reprocessing by dense gas, they differ in whether the continuum is interpreted as stellar-photosphere-like emission versus partially processed recombination radiation. For instance, de Graaff et al. (2025b) provided an empirical study with a NIRSpect/*JWST* compilation of 116 LRDs showing that their spectral continua can be reproduced with blackbodies with $T \sim 2000\text{--}6000$ K multiplied by a power law ν^n with index $n \approx \pm 3$. Such modified blackbodies are interpreted as coming from an optically-thick envelope in approximate hydrostatic equilibrium. Extending this idea, Liu et al. (2026) provided a synthetic spectral library of modified blackbodies for LRDs computed using stellar atmosphere modelling codes for models with large column densities $N_H \sim 10^{27}\text{cm}^{-2}$. By contrast, Sneppen et al. (2026) provided self-consistent, 2D radiative transfer models in which the continuum is produced by recombination emission of ionised gas (i.e. a ‘nebular’ continuum) rather than by a deeply thermalised atmosphere. Synthetic spectra from these models yields a broadly similar continuum shape to a blackbody, but with one key observable distinction being a predicted change in spectral slope at the Paschen limit. If such spectral signatures can be detected (or excluded), it would allow a probe of the degree of thermalisation of the spectra.

While the Balmer break has revealed substantial surrounding column densities of hydrogen in $n = 2$ (e.g., Inayoshi &

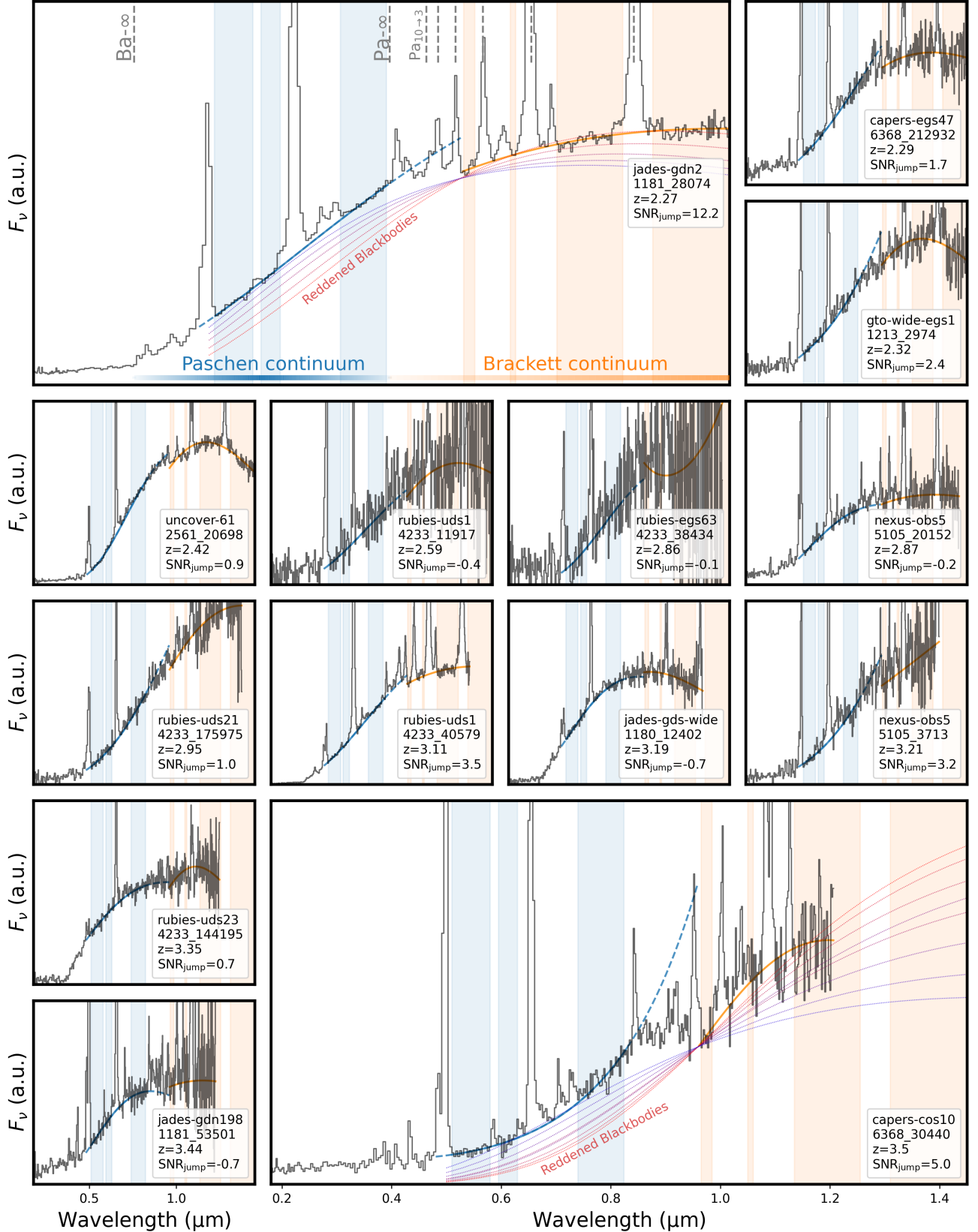


Fig. 1. *JWST* NIRSpec/PRISM sample of LRDs with polynomial fits to the spectral continuum blueward (blue) and redward (orange) of the Pa- ∞ wavelength. The LRD data and *SIRocco* recombination models show a change in spectral slope at Ba- ∞ and Pa- ∞ . Strong detected emission from high-order Paschen lines (e.g. Pa ζ), implies blended recombination-line emission immediately blueward of Pa- ∞ (i.e. $n > 10 \rightarrow n = 3$), so we fit the Brackett continuum at wavelengths with $\geq 0.96 \mu\text{m}$. For each object, we provide in the legend the SNR difference between the Paschen extrapolated continuum and the Brackett continuum, where the former typically overshoots the latter (e.g. CAPERS-6368-30440). Reddened blackbody models have a smooth curvature and cannot match the Brackett and Paschen continua simultaneously (red and blue dashed lines).

Maiolino 2025), the Paschen continuum offers complementary information by probing the intrinsic emission of the ionized cocoon, the electron temperature through free-bound emission, and the degree of external reprocessing. We therefore here explore the complementary lessons from Paschen-jump signatures in LRDs. In Sect. 2.1, we summarise the *JWST* NIRSpec/PRISM data, which include additional coverage up to $5.5 \mu\text{m}$, useful for constraining the Brackett continuum at $z \leq 3.5$. In Sect. 2.2, we show how *Sirocco* modelling motivates the expected appearance of Paschen jump signatures in the regime of strong scattering and bright Paschen recombination-line emission. In Sect. 3, we find and quantify these features of free-bound emission structures. Additionally, in Sect. 3, we discuss how pure blackbody thermalisation would require a distinct broad-line region outside the envelope photosphere. By contrast, the recombination framework in (Sneppen et al. 2026) allows a single, continuous, stratified medium to reproduce the key observables of LRDs.

2. Methods

2.1. Observations

The data used in this work were processed via the DAWN *JWST* Archive¹ (DJA) v4.4 (Brammer & Valentino 2025). The processing is described in de Graaff et al. (2025c); Heintz et al. (2025) with recent v4 improvements detailed by Pollock et al. (2025); Valentino et al. (2025). In particular, the v4 added wavelength coverage extending up to $\lambda_{\text{obs}} \sim 5.5 \mu\text{m}$, which is useful for constraining the continuum redward of the Paschen limit for the high-redshift LRD population. LRDs display strong emission features immediately redward of the Paschen limit, which necessitates wavelength coverage extending beyond $\lambda_{\text{rest}} \gtrsim 1.2 \mu\text{m}$ for strong constraints on the spectral shape. This limits the well-constrained Brackett continuum domain to the lower-redshift tail of the LRD population $z \lesssim 3.5$, while the general population is predominantly at $z \gtrsim 4$ (Kocevski et al. 2024). Therefore, here we analyse the $z \leq 3.5$ subset of the NIRSpec/PRISM LRD population using the selection of de Graaff et al. (2025b), which selected on i) the spectrum displaying an inflection near the Balmer limit and ii) being a compact source in imaging. This amounts to 14 objects with a typical resolving power of $\mathcal{R} \sim 100 - 200$ from $2.27 \leq z \leq 3.5$, see Fig. 1. In luminosity and Balmer-break strength, this low-redshift subset are representative of the broader LRD population, although it generally lacks the grating spectroscopy available for the sample compiled in our previous paper (Sneppen et al. 2026). We highlight the lowest redshift object of the sample, ‘the Rosetta Stone’ LRD (JADES 1181-28074) as it has been studied in detail (Juodžbalis et al. 2024; Brazzini et al. 2025, 2026) and provides a high signal-to-noise ratio (SNR) test of the predicted Paschen-jump structure.

2.2. *Sirocco* modelling – signatures of LRD Paschen jumps

We use the Sobolev Monte Carlo code *Sirocco* (*Simulating Ionisation and Radiation in Outflows Created by Compact Objects*; Long & Knigge 2002; Matthews et al. 2025) for radiative transfer modelling of LRDs, a problem that requires accurate treatment of electron scattering, line transfer and bound-free processes within optically thick, multi-dimensional flows (Sneppen et al. 2026). For a given input outflow structure (mass density and velocity field), *Sirocco* computes the cocoon’s radiation field and ionisation structure, thereby determining the electron

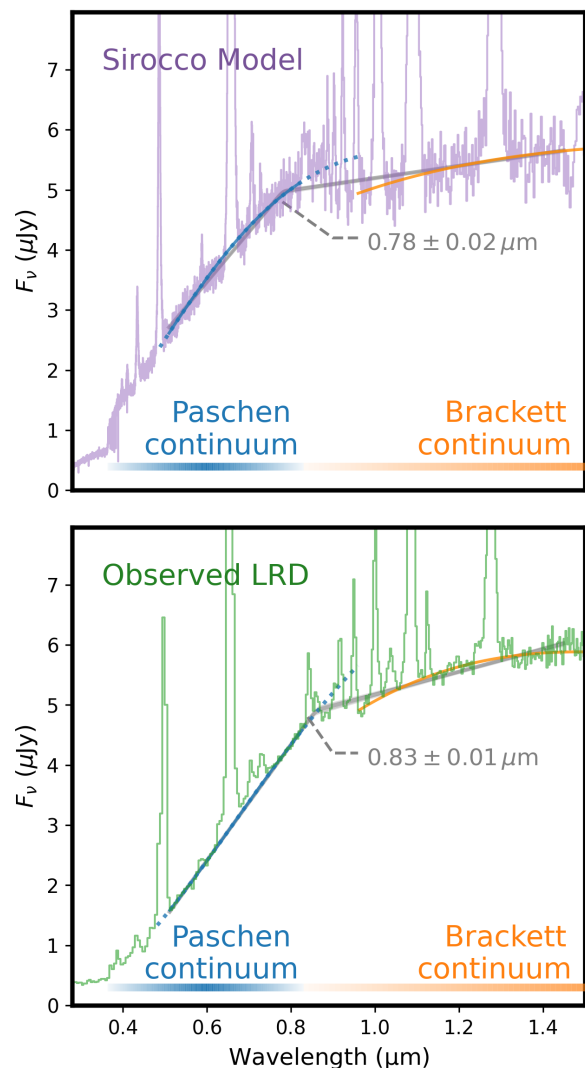


Fig. 2. Top panel: *Sirocco* LRD model highlighting the change in spectral slope expected around Pa- ∞ . Bottom panel: The Rosetta Stone LRD is shown for observational comparison. Polynomial fits to Paschen and Brackett continua are respectively indicated with blue and orange, while a piecewise linear fit to both continua displays a change in spectral slope near Pa- ∞ . Both the observed and *Sirocco* spectra show a blackbody-reminiscent continuum, despite not being thermalised, together with broad recombination lines from species with high ionisation potentials, such as He I $\lambda 1083.3 \text{ nm}$.

column density, the strength of the recombination lines and continua, the extent of partially ionised material and the strengths of Balmer and Paschen absorption lines and breaks. *Sirocco* thus permits the quantification and simultaneous reproduction of the overall spectral shapes, line profiles, line and continuum luminosities, individual absorption features, the ratios of the different lines and correlations between these quantities (Sneppen et al. 2026).

The basic geometry considered is that of a spherically symmetric cocoon with column densities of $N_H \sim 10^{25} \text{ cm}^{-2}$, outflow velocities of 100 km s^{-1} , and a central blackbody source. Here we focus on the broad-scale continua of these *Sirocco* model spectra at NIRSpec/prism resolution, for which the detailed kinematic treatment required to model grating-resolved line structure in Sneppen et al. (2026) is less important. Although that earlier analysis found evidence for non-spherical

¹ <https://dawn-cph.github.io/dja>

kinematics from the line profiles, such effects are not central to the continuum-based discussion presented here, so we adopt the simpler geometry. The resulting simulation operates using the Sobolev approximation with line transfer treated in the hybrid macro-atom limit, and computes the emerging spectrum once the ionization and temperature structure has converged under the assumption of radiative near-equilibrium. The Sirocco results and modelling are discussed in more detail by Sneppen et al. (2026), who already predicted the presence of Paschen jumps. Here we supplement the Sirocco H dataset and present two models with blackbody luminosities and temperatures of 3×10^{44} erg s⁻¹ and 20 000 K, and 10^{45} erg s⁻¹ and 100 000 K, respectively, with similar cocoon column densities. Spectra from these models are shown in Fig. 2 and Fig. 3, but these are not outliers in the simulation grid. Specifically, for high-fidelity reproduction of the Paschen structure, we expanded the fiducial atomic dataset for H in Sirocco to include all levels up to $n = 40$ using energy levels and A-values from NIST (Kramida et al. 2023) and we assume the same photoionisation cross-sections for all levels with $n \geq 20$. When applying dust extinction in this work, we use the SMC extinction curve (Gordon et al. 2003).

A notable Sirocco prediction from Sneppen et al. (2026) is that recombination emission from ionised cocoons with columns of order $N_H \sim 10^{25}$ cm⁻² – substantially below the much larger columns often invoked in fully thermalising atmosphere models – should leave a characteristic spectral imprint near $\lambda_{\text{rest}} \simeq 820$ nm (the Paschen limit, Pa- ∞). No clear step-like “jump” in flux is expected from Sirocco models; instead, the key imprint is an acute change in spectral slope across Pa- ∞ (Fig. 3). The appearance of this free-bound signature in model spectra is subtle, due to strong, broad, and blended emission immediately redward of Pa- ∞ (see Fig. 2). In the synthetic Sirocco spectra, the blended emission component is dominated by high-order Paschen lines (as discussed in AGN by Guo et al. 2022), while potential contributions from O I and Fe II emission have also been noted (Kokorev et al. 2025; Sun et al. 2026). In practice, extrapolating the Paschen (blueward) continuum to the Brackett (redward) continuum yields a mismatch in flux level, with the blue-side extrapolation overshooting the red-side continuum. Fig. 2 shows second-order polynomial fits to the Paschen and Brackett continua fitted in logarithmic space, where both models and observations display a mismatch when extrapolated across the edge. Motivated by these Sirocco expectations, we use this slope-change/mismatch as our operational signature of Paschen free-bound emission and test for it in the data.

2.3. Fitting framework

The majority of the 14 observed LRDs show Paschen-inferred continua whose extrapolation exceeds the Brackett continuum. To evaluate the significance of this excess and to provide clarity on the change in spectral slope, we explore various parametric models within a Bayesian framework. For each model, we sample the posterior distribution of the parameters using the Markov chain Monte Carlo ensemble sampler emcee (Foreman-Mackey et al. 2013), adopting uniform priors over the parameter ranges described below.

First, we provide an agnostic parametrization of the continuum blueward and redward of Pa- ∞ with a second-order polynomial fitted to the logarithmic space of wavelength and flux, $\log_{10}(F_\nu) = a \log_{10}(\lambda)^2 + b \log_{10}(\lambda) + c$, which captures curvature without imposing a physical model. This allows freedom to reproduce smooth functional rollovers or, on the other hand, to find points of sudden spectral transitions. The wavelength re-

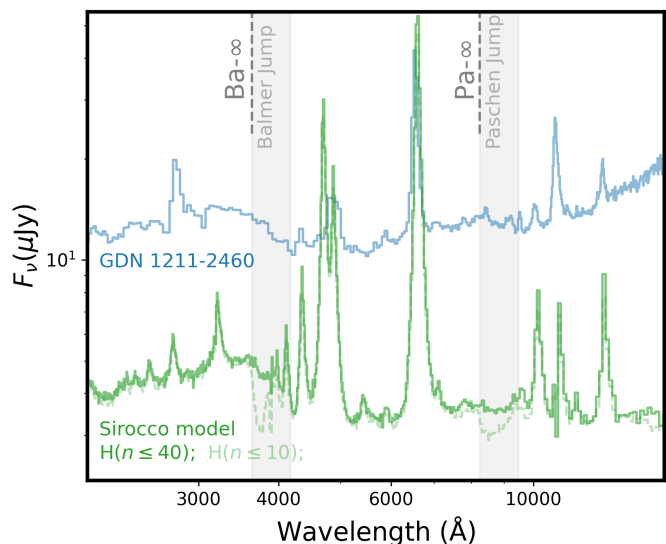


Fig. 3. A $z = 2.60$ broad-line, compact little blue dot ‘GDN 1211-2460’ (Maseda et al. 2024) displaying separated spectral slopes in the Balmer-, Paschen- and Brackett-continua. Sirocco modelling (green) with shading indicating the necessity for including $n > 10$ energy-levels of hydrogen for producing more accurate Balmer- and Paschen-jump shapes. In both the $n = 40$ model and the data, the Paschen-jump is blended with closely-spaced recombination line emission.

gions used for fitting the spectral continuum are chosen to avoid contamination from prominent known lines. We also tested the impact of excluding all wavelengths $\lambda > 1.33 \mu\text{m}$ to avoid bias from the water absorption found in two LRDs (Wang et al. 2026), but ultimately this choice does not affect our conclusions. We specifically evaluate the ratio of predicted Paschen and Brackett spectral continua at $0.95 \mu\text{m}$ as this is the shortest wavelength directly probed by the Brackett continuum before strong Paschen emission lines obscure the continuum in Sirocco models. For all LRDs, we also fit blackbody continua to the same wavelengths used for the Paschen and Brackett continua to estimate the blackbody temperature, T_{BB} . These blackbody fits provide a mean and spread in reduced chi-squared $\chi_{\nu, \text{BB}}^2 = 4.7 \pm 7.6$ compared to $\chi_{\nu, \text{poly}}^2 = 1.9 \pm 1.6$ for the polynomial parametrization. After inflating each object’s uncertainties so that the polynomial fit yields a reduced chi-square of unity, the null hypothesis that blackbody fits accurately describe the data can be ruled out in 5 (2) out of 14 objects with a significance threshold of 2σ or a p -value of 4.5% (5σ or a p -value of 5.7×10^{-5} %). Fig. 1 highlights the limitation of blackbody models to simultaneously fit the Paschen and Brackett continuum in the lowest and highest redshift objects in the sample. More generally, we emphasise that physically motivated modifications to blackbody emission can be invoked even for highly thermalised emission (e.g. H⁻ opacity kink, broader and narrower SEDs, see Liu et al. 2026), but the key observational test introduced by this paper is the sudden change in spectral slope at the Paschen limit, which is an observational difficulty for any smoothly varying thermal-like emission. In Fig. 2, we show a piecewise linear function with a free-to-vary break-position, fit simultaneously to both continua. This illustrates the expected change in spectral slope is near the Paschen limit, analogous to the change in spectral slope near the Balmer-limit.

Second, we model the continuum as a reddened PyNeb template, $F_\nu \propto C_\nu^{\text{PyNeb}}(T_e, n_e) \times 10^{-0.4A_\lambda}$, where A_λ is the extinc-

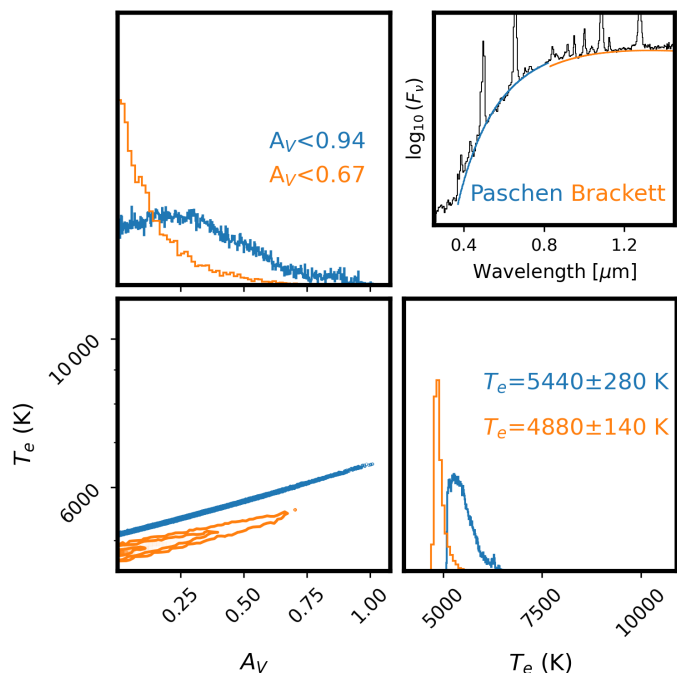


Fig. 4. Constraints on electron temperature, T_e , and dust extinction, A_V , for the Rosetta Stone from the Paschen and Brackett spectral slope assuming origin as free-bound emission with PyNEB. Top-right panel shows the corresponding $F_\nu(\lambda)$ spectral slope in PyNEB models and data. The Paschen and Brackett continua favour a modest reddening ($A_V \lesssim 0.7$, 3σ limit) and low-temperature solution, $T_e \sim 5000$ K, which was similarly required for the e-folding width found in the broad electron-scattered lines (Sneppen et al. 2026).

tion curve and C_v^{PyNeb} is the numerically evaluated continuum emissivity for a given electron temperature and density (Luridiana et al. 2015). In practice, this template represents the optically thin limit of such nebular recombination emission, rather than a full self-consistent radiative-transfer model such as in Sirocco. Under this assumption, and adopting a prior of $n_e \in [10^6 - 10^{10}] \text{cm}^{-3}$, we can extract the electron temperature and dust reddening from the continuum’s spectral slope. In optically thin conditions, the Paschen jump prominence is a strong complementary diagnostic of electron temperature as it is a local emissivity diagnostic. However, the jump prominence is obscured in the Sirocco models both observationally, due to strong emission of blended Paschen lines, and intrinsically as in optically thick conditions not only the emission coefficient, j_ν , but also the absorption coefficient, κ_ν , changes over the Paschen limit. Thus, in the Sirocco models, while the microscopic opacity/emissivity edge still exists, the emergent discontinuity from the source function $S_\nu = j_\nu/\kappa_\nu$ is weak and perhaps only clearly apparent when removing the atomic levels that contribute the emissivity just above the Paschen limit (see $n \leq 10$ in Fig. 3).

3. Results

4 of 14 objects show a significant deviation from a smooth rollover at $> 3\sigma$ significance with the Paschen continuum extrapolation lying consistently above the Brackett continuum (see legend in Fig. 1 or Fig. 5). Notably, this includes a 12σ outlier in a relatively modest sample size of objects. This is the Rosetta Stone LRD, which has the highest continuum SNR in the sample with $\text{SNR}_{1.2\mu\text{m}} \approx 100$, so we highlight this in the top panel of Fig. 1 where, for comparison, multiple blackbodies of varying

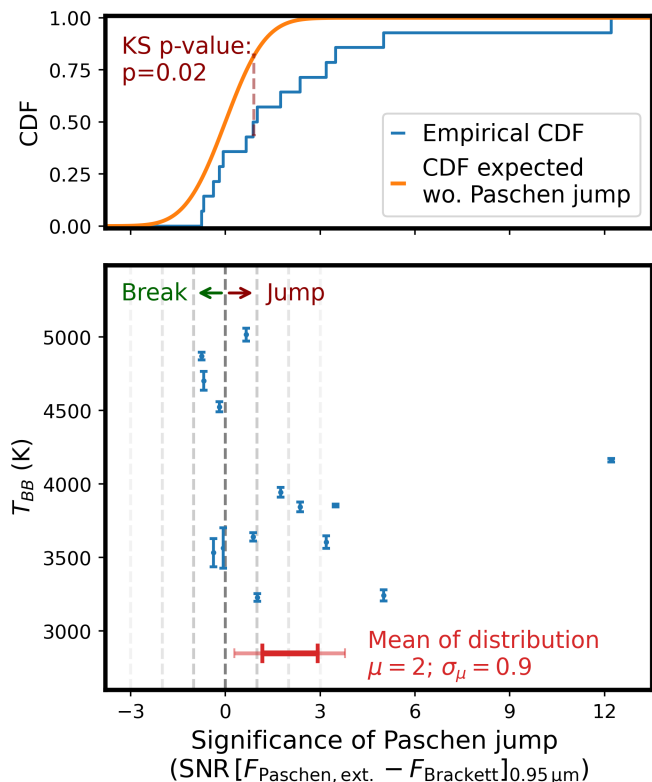


Fig. 5. Spectra display systematic evidence for a Paschen jump, quantified from the difference between Paschen- and Brackett-extrapolated continua at $0.95 \mu\text{m}$. Bottom panel: for each object, the associated SNR is estimated from posterior samples of the continuum fits (uncertainties from the 16th–84th percentile range at $0.95 \mu\text{m}$) and plotted against best-fit blackbody temperature. 4 out of 14 objects show Paschen jump signatures at $> 3\sigma$. Top panel: cumulative distribution function (CDF) of the significance of jumps (blue) compared to the null expectation in the absence of a Paschen-jump signature (orange). The Kolmogorov–Smirnov (KS) test indicates the two distributions are inconsistent with being drawn from the same parent distribution ($p < 0.05$).

temperature and subject to differing levels of dust reddening are shown. Although simple blackbody emission can reproduce the Brackett continuum or the very bluest Paschen continuum emission, they cannot smoothly fit both wavelength regimes. Most objects consistent with smooth rollovers comes from the lower SNR part with none of the 5 objects with $\text{SNR}_{1.2\mu\text{m}} > 10$ (useful to constrain the Brackett continuum) is consistent with smooth rollover within 1σ , and in all cases because the Paschen extrapolation overshoots the Brackett continuum.

While a Paschen jump signature is inconsistent with the null hypothesis of cold thermalised blackbody continuum, we emphasise that an apparently smooth rollover (i.e. the absence of a clear Paschen jump) is not inconsistent with direct recombination emission in the partially optically thick regime seen in Sirocco models. However, plotting the significance of a Paschen spectral break versus the best-fit blackbody temperature in Fig. 5, four $T_{\text{BB}} \gtrsim 5000$ K LRDs are consistent with a smooth rollover. These resemble the ‘Cliff’-like LRDs (de Graaff et al. 2025a). If interpreted literally as blackbody temperatures, these T_{BB} values fall in a regime where H^- -opacity can be efficient in stellar atmospheres, potentially producing pseudo-thermalised continua. Reproducing blackbody-adjacent contin-

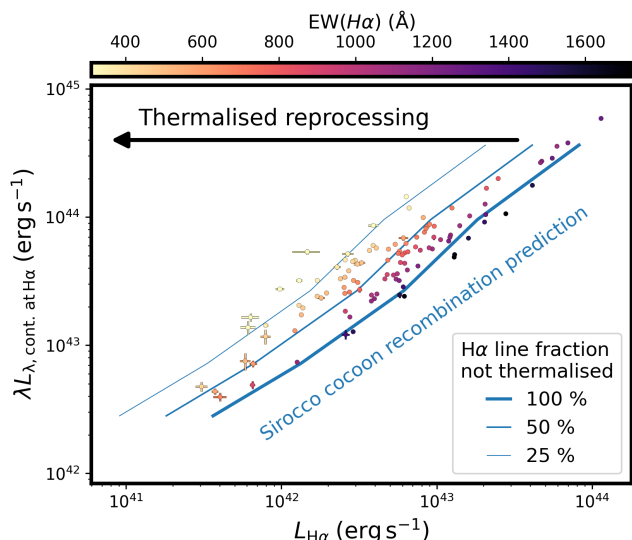


Fig. 6. Comparison of $H\alpha$ line (integrated above the continuum) and the continuum luminosity at $H\alpha$ -wavelength for the 116-object LRD sample from de Graaff et al. (2025b). In the Sirocco model sequence from Fig. 3 of Sneppen et al. (2026) (thick blue curve), these quantities are tightly linked because both the continuum and the line emission arise from recombination processes (respectively free-bound recombination and recombination cascades). Any additional blackbody-like reprocessing moves objects away from this relation by reducing the emergent line luminosity relative to the optical continuum; the offset increases with the assumed fraction level of reprocessing (thinner blue curves). In the limit of a highly optically thick envelope and a thermalised blackbody outside the line-forming region, the continuum-subtracted $H\alpha$ line luminosity, $L_{H\alpha}$, tends to zero, because the thermalised continuum is not itself hot enough for the requisite photoionisation.

uum shapes may motivate the inclusion of H^- -opacity within Sirocco in the future.

3.1. Spectral slope constraints on T_e

Using the nebular code PYNEB to fit the electron-temperature, T_e , we find that the detailed shape of the Paschen continuum and the overall rise toward the Paschen series limit are consistent with $T_e \lesssim 10^4$ K and low reddening, $A_V \lesssim 1$, across the sample. For instance, for the Rosetta Stone, the Paschen and Brackett continuum slopes would independently suggest 5400 ± 300 K and 4900 ± 100 K respectively for a flat prior on the dust-extinction up to $A_V = 5$ (see Fig. 4). The dust extinction from this estimate is $A_V \lesssim 0.7 - 1$ mag as a 3σ upper limit, which is modest in comparison to stellar UV fits and narrow Balmer line-ratios assuming case B recombination (respectively, $A_V \sim 0.68$ and $A_V = 1.1 \pm 0.1$, Juodžbalis et al. 2024), although we note other opacity sources or emission components could bias the spectral shape. Generally, across the sample the inferred T_e and A_V are strongly degenerate as they similarly steepen the spectral slope (Guseva et al. 2006). Using that the minimal Balmer decrement is that of Case B recombination ratios, one can invoke a prior on A_V with an upper-limit ranging from $A_V \sim 1$ to $A_V \sim 5.2$ depending on the object in the sample. Invoking this prior means all five well-constrained objects are only consistent with $T_e \leq 10^4$ K. While the remaining objects permit a broader family of reddening and temperatures, none are inconsistent with $T_e \leq 10^4$ K.

In reality, there is likely to be some stratification in temperature within the cocoon, as is indeed found in the Sirocco models. However, the modest gas temperatures from our sin-

gle temperature model are consistent with those implied by Fe II emission (~ 7000 K, Torralba et al. 2025), Ca triplet absorption (~ 5000 K, Lin et al. 2025) and electron-scattering widths (~ 5000 K, Sneppen et al. 2026). This consistency with the electron-scattering widths indicates that the recombining gas responsible for producing the continuum and the gas responsible for the line-broadening share similar thermodynamic conditions. This, in turn, strengthens the argument that the line-forming region is approximately co-spatial with the continuum-emitting region.

3.2. A test of thermalised reprocessing – $EW(H\alpha)$

The LRD population shows a tight relation between continuum luminosity and hydrogen line emission (de Graaff et al. 2025b; Pang et al. 2026), as predicted by our radiative-transfer models, because both the continuum and lines arise from recombination emission in the same general gas region (see Fig. 6). From this perspective, we also caution against interpreting the emission as a true *blackbody*. Strong hydrogen recombination lines are produced in the inner, ionised cocoon, whereas the continuum may subsequently undergo additional reprocessing in cooler, partially ionised outer layers mediated by H^- -opacity. Because the continuum is already smooth and thermal-like, additional absorption and re-emission in optically thick outer layers would mostly preserve its broad spectral character. By contrast, line emission is initially concentrated into spectral features, so repeated reprocessing would tend to convert part of that line luminosity into a smoother continuum-like component. If the outer layers became sufficiently optically thick to thermalise the radiation field, the emergent spectrum seen by an external observer would therefore show diluted line features, even though the continuum luminosity is similar. In that limit, the observable coupling between line strength and continuum luminosity is reduced in proportion to the assumed level of reprocessing/thermalisation.

The line-to-continuum ratio, $EW(H\alpha) = L_{H\alpha}/L_{\lambda,\text{cont.at.H}\alpha}$, is high, reaching equivalent widths of $EW(H\alpha)_{\text{LRD}} = 1700 \pm 100$ Å, well above the expectation from standard AGN relations (i.e. $EW(H\alpha)_{\text{AGN}} \sim 200$ Å, Greene & Ho 2005; Maiolino et al. 2025). The prominent jump in an object like CAPERS 6368-30440 is consistent with direct line emission with $EW(H\alpha) = 1500 \pm 60$ Å, while the subtler jump in the Rosetta Stone with $EW(H\alpha) = 820 \pm 6$ Å may indicate modest reprocessing to the continuum. For comparison, the thick blue line in Fig. 6 shows this luminosity relation in the Sirocco model sequence from Sneppen et al. (2026), in which the density is varied up to a Balmer-break strength of $D_{4000} = F_{\lambda=4200\text{Å}}/F_{\lambda=3500\text{Å}} = 20$. Any additional thermalisation in exterior layers would not dramatically change the continuum colours and would mainly act to weaken the apparent line emission relative to the continuum by a factor of a few. We indicate the approximate scale of this effect with thinner blue lines, which are simple offsets from the main Sirocco relation rather than separately computed models.

Thus, both i) the tight observed correlation and ii) the high equivalent width found in LRDs suggest that thermalisation processes in any putative stellar atmosphere are limited and does not fully reprocess the incident emission. Even the strongest outliers from the fiducial Sirocco recombination emission relation are at most a factor of few underluminous in the $H\alpha$ line, such as objects like ‘the Cliff’. Alternatively, broad-lines superposed on a thermalised continuum could be produced if the broad permitted lines were formed outside the black hole envelope; however, this would require an ionizing energy source distinct from the

AGN that is producing the optical-IR continuum (e.g. Inayoshi et al. 2025), or would necessitate an inverted temperature structure with a highly ionised exterior. Furthermore, given the strong correlation between lines and continuum, such a scenario would require the energetic source outside the envelope to be closely tuned to the SMBH's accretion luminosity. In addition, the observed $H\alpha$ EW is already very large, so invoking a substantial continuum contribution from any component other than the line-emitting region would require an even more extreme intrinsic EW in that region. Lastly, given that the electron scattering and absorption is acting on broad H and He lines, it would also still require this external broad-line component to lie within some extended high-column density envelope, which also has a T_e very similar to that of the continuum.

3.3. A single nebular component producing lines and continua

A key success of the Sirocco LRD spectra is thus their ability to reproduce the continuum, line strengths and line profiles simultaneously, without requiring multiple separately fitted components. The model naturally produces a thermal-looking optical continuum, with $k_B T_{BB} \sim 0.3$ eV, while also predicting recombination lines from species requiring much higher ionization energies deeper within the cocoon, such as $Ly\alpha$, $H\alpha$ and $He I$ $\lambda 1083.3$ nm. Moreover, the column density implied by the Balmer break agrees with that inferred from electron-scattering broadening (Sneppen et al. 2026). Likewise, the electron temperature inferred from the continuum shape agrees, without fine-tuning, with that inferred from scattering-broadened line widths.

Acknowledgements

The Sirocco code (Matthews et al. 2025) and documentation are publicly available². The comparison to observed LRD makes use of the public *JWST* data collected as part of several observational programs with the NIRSpec spectrograph (Jakobsen et al. 2022) as enumerated in the original sample paper by de Graaff et al. (2025b) with the following PIDs; (CANUCS Sarrouh et al. 2026); 6368 (CAPERS); 1345 (CEERS Finkelstein et al. 2025); 2750 (PI: Arrabal Haro); 2767 (PI: Kelly); 6585 (PI: Coulter); 1433 (PI: Coe); 2198 (PI: Barrufet); 4106 (PIs: Nelson and Labbe); 1211, 1212, 1213, 1215 (GTO-WIDE Maseda et al. 2024); 1180, 1181, 1286 (JADES Eisenstein et al. 2023; Bunker et al. 2024; D'Eugenio et al. 2025b; Arrabal Haro et al. 2021); 4233 (RUBIES de Graaff et al. 2025c); 5224 (MoM Naidu et al. 2025); 5105 (5105 Shen et al. 2024); 2561 (2561 Bezanson et al. 2024; Price et al. 2025). These observations have been uniformly reduced and published as part of the Dawn *JWST* Archive³ (DJA), de Graaff et al. (2025c); Heintz et al. (2025); Pollock et al. (2025). DJA is an initiative of the Cosmic Dawn Center (DAWN), which is funded by the Danish National Research Foundation under grant DNR140. AS, DW and KEH acknowledge funding by the European Union (ERC, HEAVYMETAL, 101071865). Views and opinions expressed are, however, those of the authors only and do not necessarily reflect those of the European Union or the European Research Council. Neither the European Union nor the granting authority can be held responsible for them. JHM acknowledges funding from a Royal Society University Research Fellowship (URFR1221062). SAS were sup-

ported by the UK's Science and Technology Facilities Council (STFC, respectively grant ST/V001000/1 and ST/X00094X/1).

References

- Arrabal Haro P., et al., 2021, Environmental effects on galaxy evolution in a $z=5.2$ proto-cluster, *JWST Proposal*. Cycle 1, ID. #2674
- Begelman M. C., Dexter J., 2025, *arXiv e-prints*, p. [arXiv:2507.09085](https://arxiv.org/abs/2507.09085)
- Bezanson R., et al., 2024, *ApJ*, **974**, 92
- Brammer G., Valentino F., 2025, The DAWN *JWST* Archive: Compilation of Public NIRSpec Spectra, [doi:10.5281/zenodo.15472354](https://doi.org/10.5281/zenodo.15472354), <https://doi.org/10.5281/zenodo.15472354>
- Brazzini M., D'Eugenio F., Maiolino R., Juodžbalis I., Ji X., Scholtz J., 2025, *arXiv e-prints*, p. [arXiv:2507.08929](https://arxiv.org/abs/2507.08929)
- Brazzini M., et al., 2026, *arXiv e-prints*, p. [arXiv:2601.22214](https://arxiv.org/abs/2601.22214)
- Bunker A. J., et al., 2024, *A&A*, **690**, A288
- Chang S.-J., Gronke M., Matthee J., Mason C., 2025, *arXiv e-prints*, p. [arXiv:2508.08768](https://arxiv.org/abs/2508.08768)
- D'Eugenio F., et al., 2025a, *arXiv e-prints*, p. [arXiv:2510.00101](https://arxiv.org/abs/2510.00101)
- D'Eugenio F., et al., 2025b, *ApJS*, **277**, 4
- Eisenstein D. J., et al., 2023, *arXiv e-prints*, p. [arXiv:2306.02465](https://arxiv.org/abs/2306.02465)
- Finkelstein S. L., et al., 2025, *ApJ*, **983**, L4
- Foreman-Mackey D., Hogg D. W., Lang D., Goodman J., 2013, *PASP*, **125**, 306
- Gordon K. D., Clayton G. C., Misselt K. A., Landolt A. U., Wolff M. J., 2003, *ApJ*, **594**, 279
- Greene J. E., Ho L. C., 2005, *ApJ*, **630**, 122
- Greene J. E., et al., 2024, *ApJ*, **964**, 39
- Guo H., et al., 2022, *ApJ*, **927**, 60
- Guseva N. G., Izotov Y. I., Thuan T. X., 2006, *ApJ*, **644**, 890
- Heintz K. E., et al., 2025, *A&A*, **693**, A60
- Inayoshi K., Maiolino R., 2025, *ApJ*, **980**, L27
- Inayoshi K., Murase K., Kashiyama K., 2025, *arXiv e-prints*, p. [arXiv:2509.19422](https://arxiv.org/abs/2509.19422)
- Jakobsen P., et al., 2022, *A&A*, **661**, A80
- Juodžbalis I., et al., 2024, *MNRAS*, **535**, 853
- Kido D., Ioka K., Hotokezaka K., Inayoshi K., Irwin C. M., 2025, *arXiv e-prints*, p. [arXiv:2505.06965](https://arxiv.org/abs/2505.06965)
- Killi M., et al., 2024, *A&A*, **691**, A52
- Kocevski D. D., et al., 2024, *arXiv e-prints*, p. [arXiv:2404.03576](https://arxiv.org/abs/2404.03576)
- Kokorev V., et al., 2024, *ApJ*, **968**, 38
- Kokorev V., et al., 2025, *arXiv e-prints*, p. [arXiv:2511.07515](https://arxiv.org/abs/2511.07515)
- Kramida A., Ralchenko Y., Reader J., Team N. A., 2023, NIST Atomic Spectra Database, [doi:10.18434/T4W30F](https://physics.nist.gov/asd), <https://physics.nist.gov/asd>
- Lin X., et al., 2025, *arXiv e-prints*, p. [arXiv:2507.10659](https://arxiv.org/abs/2507.10659)
- Liu H., Jiang Y.-F., Quataert E., Greene J. E., Ma Y., 2025, *ApJ*, **994**, 113
- Liu H., Jiang Y.-F., Quataert E., Greene J. E., Ma Y., Lin X., 2026, *arXiv e-prints*, p. [arXiv:2603.02317](https://arxiv.org/abs/2603.02317)
- Long K. S., Knigge C., 2002, *ApJ*, **579**, 725
- Luridiana V., Morisset C., Shaw R. A., 2015, *A&A*, **573**, A42
- Maiolino R., et al., 2025, *MNRAS*,
- Maseda M. V., et al., 2024, *A&A*, **689**, A73
- Matthee J., et al., 2024, *ApJ*, **963**, 129
- Matthews J. H., et al., 2025, *MNRAS*, **536**, 879
- Naidu R. P., et al., 2025, *arXiv e-prints*, p. [arXiv:2503.16596](https://arxiv.org/abs/2503.16596)
- Nikopoulos G. P., Watson D., Sneppen A., Rusakov V., Heintz K. E., Witstok J., Brammer G., 2025, *arXiv e-prints*, p. [arXiv:2510.06362](https://arxiv.org/abs/2510.06362)
- Pang Y., Wang X., Cheng C., Wang S., Zhou H., Zhou Q., Wu X.-B., Glazebrook K., 2026, *arXiv e-prints*, p. [arXiv:2602.12548](https://arxiv.org/abs/2602.12548)
- Pollock C. L., et al., 2025, *arXiv e-prints*, p. [arXiv:2506.15779](https://arxiv.org/abs/2506.15779)
- Price S. H., et al., 2025, *ApJ*, **982**, 51
- Rusakov V., et al., 2026, *Nature*, **649**, 574
- Sarrouh G. T. E., et al., 2026, *ApJS*, **282**, 3
- Setton D. J., et al., 2024, *arXiv e-prints*, p. [arXiv:2411.03424](https://arxiv.org/abs/2411.03424)
- Shen Y., et al., 2024, *arXiv e-prints*, p. [arXiv:2408.12713](https://arxiv.org/abs/2408.12713)
- Sneppen A., et al., 2026, *arXiv e-prints*, p. [arXiv:2601.18864](https://arxiv.org/abs/2601.18864)
- Sun W. Q., et al., 2026, *arXiv e-prints*, p. [arXiv:2601.20929](https://arxiv.org/abs/2601.20929)
- Torralba A., et al., 2025, *arXiv e-prints*, p. [arXiv:2510.00103](https://arxiv.org/abs/2510.00103)
- Valentino F., et al., 2025, *A&A*, **699**, A358
- Wang B., et al., 2026, *arXiv e-prints*, p. [arXiv:2602.06024](https://arxiv.org/abs/2602.06024)
- Yan Z., Inayoshi K., Chen K., Guo J., 2025, *arXiv e-prints*, p. [arXiv:2512.11050](https://arxiv.org/abs/2512.11050)
- de Graaff A., et al., 2025a, *arXiv e-prints*, p. [arXiv:2503.16600](https://arxiv.org/abs/2503.16600)
- de Graaff A., et al., 2025b, *arXiv e-prints*, p. [arXiv:2511.21820](https://arxiv.org/abs/2511.21820)
- de Graaff A., et al., 2025c, *A&A*, **697**, A189

² <https://github.com/sirocco-rt/sirocco>

³ <https://dawn-cph.github.io/dja>